Metal Ion Binding to Human Hemopexin†

Marcia R. Mauk,‡ Federico I. Rosell,‡ Barbara Lelj-Garolla,‡ Geoffrey R. Moore,§ and A. Grant Mauk*,‡

Department of Biochemistry and Molecular Biology and Centre for Blood Research, University of British Columbia, Vancouver, British Columbia V6T 1Z3, Canada, and School of Chemical Sciences and Pharmacy, University of East Anglia, Norwich NR7 4TJ, U.K.

Received August 24, 2004; Revised Manuscript Received November 8, 2004

ABSTRACT: Binding of divalent metal ions to human hemopexin (Hx) purified by a new protocol has been characterized by metal ion affinity chromatography and potentiometric titration in the presence and absence of bound protoheme IX. ApoHx was retained by variously charged metal affinity chelate resins in the following order: $Ni^{2+} > Cu^{2+} > Co^{2+} > Zn^{2+} > Mn^{2+}$. The Hx−heme complex exhibited similar behavior except the order of retention of the complex on Zn^{2+}- and Co^{2+}-charged columns was reversed. One-dimensional ^1H NMR of apoHx in the presence of Ni^{2+} implicates at least two His residues and possibly an Asp, Glu, or Met residue in Ni^{2+} binding. Potentiometric titrations establish that apoHx possesses more than two metal ion binding sites and that the capacity and/or affinity for metal ion binding is diminished when heme binds. For most metal ions that have been studied, potentiometric data did not fit to binding isotherms that assume one or two independent binding sites. For Mn^{2+}, however, these data were consistent with a high-affinity site [$K_A = (15 \pm 3) \times 10^6$ M^{-1}] and a low-affinity site ($K_A \leq 2 \times 10^3$ M^{-1}). Binding of Cu^{2+} and Zn^{2+} to the Hx−heme complex produced significant changes in the Soret-CD spectrum of the Hx−heme complex that were reversed with addition of EDTA. Possibly, these metal ions bind near the heme binding site and perturb the electronic environment of the heme, or their binding induces exchange of one axial His ligand to the heme iron with another adjacent His residue. A possible role for Hx in the maintenance of metal ion homeostasis is discussed.

Hemopexin (EC 3.2.1.35) is a plasma protein that binds heme that is released to plasma as the result of hemolysis or tissue damage. The protein circulates normally as apohemopexin and is cleared quickly from circulation by the liver following heme binding. The apoprotein is then returned to circulation (*1*, *2*). In addition to reducing the extent of iron loss, scavenging of heme by hemopexin is believed to prevent oxidative damage that can result from the oxidative catalytic activity of free heme (*3*, *4*). The physiological roles (*5*, *6*) and heme binding properties (*7*) of hemopexin have been reviewed recently, and the three-dimensional structure of the rabbit hemopexin−heme complex has been determined to a resolution of 2.3 Å for the deglycosylated protein (*8*).

Previous studies of hemopexin have emphasized either the physiological role of the protein (*5*, *6*, *9*) or the thermodynamics and kinetics of heme binding (*7*, *10*−*12*). One aspect of hemopexin function that has not been considered in detail, however, is its ability to bind non-heme metal ions. This facet of hemopexin function was first recognized by Porath and Olin when they discovered that immobilized metal-affinity chromatography (IMAC) could be used to separate several metal-binding plasma proteins, including hemopexin [on Ni^{2+}−tris(carboxymethyl)ethylenediamine−Sepharose 4B (*13*)]. Although this finding was confirmed in subsequent chromatographic studies (*14*−*18*), no practical method for hemopexin purification by IMAC has been developed, and no characterization of metal ion binding to hemopexin has been reported. In the current study, we have developed an efficient IMAC method for purifying human hemopexin from a plasma byproduct of blood processing and have performed an initial survey of metal ion binding to hemopexin.

EXPERIMENTAL PROCEDURES

Hemopexin Purification. Frozen samples of the cryosupernatant fraction of human plasma that were prepared under sterile conditions and subjected to standard screening procedures for pathogens were obtained in sealed plastic bags from Canadian Blood Services. Each unit (∼200 mL) was thawed by placing the sealed bag in water at room temperature. As soon as the cryosupernate was thawed, PMSF (0.26 g in 8 mL of ethanol) was added in a dropwise fashion. The resulting solution was depleted of lipids by extraction (for 30 min) with an equal volume of a mixture of diisopropyl ether and 1-butanol (3:2, v/v) (*19*). The aqueous phase was retained and diluted 8-fold with ice-cold distilled water and loaded onto a column (5 cm × 15 cm) of DE52 cellulose

† This work was supported by Canadian Institutes of Health Research Operating Grant MOP-53131 (A.G.M.), a Canada Research Chair (A.G.M.), a UBC Paetzold Family Graduate Studentship (B.L.-G.), and a travel grant from the Royal Society (G.R.M.). The analytical ultracentrifuge, the 600 MHz NMR spectrometer, and the Äkta chromatography system were obtained with funds provided by the Canadian Foundation for Innovation to the University of British Columbia Laboratory of Molecular Biophysics and the University of British Columbia Centre for Blood Research, respectively.

* To whom correspondence should be addressed: Department of Biochemistry and Molecular Biology, Life Sciences Centre, 2350 Health Sciences Mall, University of British Columbia, Vancouver, BC V6T 1Z3, Canada. Telephone: (604) 822-3719. Fax: (604) 822-6860. E-mail: mauk@interchange.ubc.ca.

‡ University of British Columbia.

§ University of East Anglia.

10.1021/bi0481747 CCC: $30.25
Published on Web 01/22/2005

(Whatman) that had been equilibrated at 4 °C with buffer A [10 mM sodium phosphate buffer (pH 7.4)]. The column was washed with this buffer until the eluant exhibited an absorbance at 280 nm of <0.3 (path length, 1 cm). The column was then developed with a linear gradient of sodium chloride (from 0 to 300 mM NaCl in 800 mL of buffer A). Fractions collected prior to 50 mM NaCl were pooled in 45 mL volumes, and NaCl (1.31 g) was added to each. After the pH was adjusted to 7.4, these protein solutions were first subjected to IMAC at 25 °C on a 5 mL HiTrap chelating HP column (Amersham) that had been saturated with $ZnSO_4$ and equilibrated with buffer B [20 mM sodium phosphate buffer and 500 mM NaCl (pH 7.4)]. Bound proteins were eluted with an imidazole gradient in buffer B. Hx-containing fractions from Zn^{2+}-HiTrap were diluted 3-fold with buffer B before a second IMAC step on a $NiCl_2$-saturated HiTrap column. Only Hx without heme (apoHx) was isolated in our procedure. ApoHx eluted at 15−40 and 60−135 mM imidazole from the Zn^{2+}- and Ni^{2+}-HiTrap columns, respectively. All IMAC separations were performed with an Äkta Purifier chromatography system, and all imidazole used for IMAC was recrystallized from toluene to minimize its absorbance at 280 nm.

The purified apoHx was exchanged into 20 mM sodium phosphate buffer (pH 7.4) by ultrafiltration (Amicon Ultra, Millipore), and 1.5 equiv of Fe(III)-protoporphyrin IX (Frontier Scientific) was added.[1] After incubation for 16 h on ice, NaCl was added to a final concentration of 500 mM, and the pH was adjusted to 7.4. This solution was rechromatographed on a Ni^{2+}-saturated HiTrap column as before with the Hx−heme complex eluting as a single peak at 20−50 mM imidazole. Yields of 30−60 mg of Hx, based on a molar absorptivity at 280 nm of 123 000 M^{-1} cm^{-1} for apoHx (ExPaSy, ProtParamTool) and 136 000 M^{-1} cm^{-1} for the Hx−heme complex (*20*), were obtained per unit of cryosupernate. This variation in yield presumably reflects individual variation in the Hx content of blood samples. Hx preparations were frozen in liquid nitrogen and stored at −80 °C.

The A_{414}/A_{280} ratio for the Hx−heme complex isolated by this method was typically 0.94−1.0 (20 mM sodium phosphate buffer at pH 7.2 and 25 °C). SDS−PAGE in 10% gels revealed a single broad band at a MW of 58000−65000 under nonreducing conditions or a MW of 73000−80000 under reducing conditions.

Analytical Ultracentrifugation. The state of aggregation of samples of the Hx−heme complex (6.5 μM) was analyzed by sedimentation velocity (50 000 rpm, 20 °C) with a Beckman Optima XL-I analytical ultracentrifuge (model An-60Ti rotor) using 12 mm standard aluminum double-sector centerpieces and quartz windows. Protein samples were prepared in sodium phosphate buffer (20 mM and pH 7.2), and the same buffer was used in the reference sector of the centerpiece. Radial scans monitored at 414 nm were acquired with no interval set between scans and with radial steps of 0.003 cm in continuous mode. The resulting data were analyzed as a $c(s)$ distribution of Lamm equation solutions with SEDFIT (*21*). Solvent density (1.00077 g/L) was calculated with SEDNTERP (*22*) as modified by J. Philo (http://www.jphilo.mailway.com/download.htm), and a partial specific volume for the (glycosylated) Hx−heme complex of 0.702 mL/g (*20*) was used.

Potentiometric Titrations. The binding of Zn^{2+}, Co^{2+}, Ni^{2+}, Mn^{2+}, and Cu^{2+} to apoHx and the Hx−heme complex was studied potentiometrically at 25 °C according to the method of Laskowski and Finkenstadt (*23*) with a computer-controlled Radiometer ABU93 Triburet as described previously (*24*). Radiometer glass (pHG201) and reference (XR130) electrodes were used to measure pH. Before titrations, protein solutions were transferred into 20 mM sodium phosphate buffer, 10 mM EDTA, and 100 mM NaCl (pH 7.3) and then exchanged into 50 mM NaCl (pH 7.2) by centrifugal ultrafiltration (Amicon Ultra, 30000 NMWL). Protein and titrant solutions were flushed extensively with Ar to remove dissolved CO_2, and the titrator vessels and tubing were washed with 5 mM HCl and 0.1 M KCl to remove adsorbed metals. Atomic absorption metal standards (Zn^{2+}, Co^{2+}, Mn^{2+}, and Cu^{2+} from Titrisol, EM Science; Ni^{2+} from VWR) were diluted with a NaCl solution to a final ionic strength of 50 mM.

Titration curves that were collected consist of 50−80 points that correspond to the volume of standardized acid or base required to re-establish the starting pH of a 2.5 mL solution of Hx (9.90−11.49 μM) after each microaddition of metal solution. These data are expressed in terms of the mole fraction of exchanged protons, H_e^+, versus the [metal^{2+}]/[Hx] ratio from which association constants (K_a) and the saturating value of H_e^+, q, can be obtained by nonlinear regression analysis with Scientist (MicroMath) as described previously (*25*).

NMR Spectroscopy. NMR spectra of apo- and holoHx were measured with Varian Unity Inova 500 and 600 MHz spectrometers at 25 °C unless otherwise specified. Proton chemical shifts were measured from the HOD peak at 4.75 ppm. One-dimensional ^{1}H NMR spectra were acquired with spectral windows of 30000−200000 Hz and with a Super-WEFT pulse sequence (*26*) or presaturation of the residual solvent resonance. A τ value of 50 ms, acquisition times of 25−167 ms, and repetition rates of 75−217 ms were used for the Super-WEFT experiments. The saturation periods for the presaturation experiments were 500−2000 ms. Line-broadening functions of 10−60 Hz were used prior to Fourier transformation, and baselines were corrected by first fitting the spectrum to a sinusoidal function and then applying a multipoint baseline correction algorithm implemented in Grams 7AI (Thermo Galactic). Samples for NMR were treated with EDTA (see Potentiometric Titrations) and then exchanged into final solution conditions by ultracentrifugation. Samples were 0.3−0.5 mM protein in 50 mM sodium chloride and in 99.99% ^2H_2O or a 10% ^2H_2O/90% ^1H_2O mixture at pH 7.0. Quoted pH values were direct meter readings uncorrected for any isotope effect. Added metal ion solutions were dilutions of $NiCl_2$ and $CoCl_2$ atomic absorption standards.

Electronic and CD Spectroscopy. Electronic absorption spectra were recorded with a Cary 6000i UV−vis spectrophotometer. Circular dichroism measurements were performed with a Jasco J-720 or J-810 spectropolarimeter to monitor the spectroscopic influence of various metal ions

[1] All references to heme in this report refer to ferriprotoheme IX. Subsequent discussion of published studies of the Hx−heme complex is similarly restricted to those concerning ferriprotoheme IX.

(Zn^{2+}, Co^{2+}, Ni^{2+}, Mn^{2+}, and Cu^{2+}) on hemopexin. These CD spectra represent the average of four scans and were collected with either a 1 or a 0.1 cm quartz cuvette. Protein samples (~8 μM holoHx) were prepared in 50 mM bisTris buffer and 50 mM NaCl (pH 7.0), and all spectra were recorded at 25 °C.

RESULTS

Hemopexin Purification. The method described above allows rapid purification of hemopexin from large quantities of cryosupernate. By avoiding dialysis, protein precipitation steps, and significant changes in pH, we minimize problems with protein cleavage and polymerization (*27*−*30*) that have been issues with previously published methods. The lipid extraction step in our procedure had no detectable effect on the properties of the hemopexin isolated and was instituted to eliminate channeling in the DE-52 resin during the sodium chloride gradient elution. DE-52 chromatography allows a first stage separation based on pI. This step is followed by IMAC column chromatography that employs selectivity based on affinity for Zn^{2+} and Ni^{2+} ions. The IgG and α_2-macroglobulin that often copurify with hemopexin (*13*, *14*, *16*, *17*) are resolved from apoHx during the Ni^{2+}-HiTrap imidazole gradient chromatography. In the final Ni^{2+}-HiTrap chromatography step for purification of the Hx−heme complex, gradient conditions were identical to those used for apoHx. The Hx−heme elution is well-resolved from the apoHx position, and unbound heme is retained on the Ni^{2+}−HiTrap column under our gradient elution conditions.

Hemopexin exhibits a broad band on SDS−PAGE which is most likely a reflection of the Hx−carbohydrate heterogeneity. In agreement with studies of sheep (*31*) and human (*32*) Hx, the five N-linked and one O-linked glycans in human hemopexin (*33*) probably produce subcomponents of Hx possessing different numbers of sialic acid residues. Our purified hemopexin is comprised of at least five components with pI values ranging from 5.46 to 6.36 as indicated by analysis with the Beckman-Coulter ProteomeLab PF2D system (data not shown).

Sedimentation Velocity Measurements. The oligomerization state of hemopexin was evaluated by modeling the sedimentation boundaries observed in the sedimentation velocity experiments as a superimposition of finite elements of the Lamm equation for noninteracting species with SEDFIT (*21*). The resulting distribution functions of sedimentation coefficients $c(s)$ for early and late eluting fractions of the Hx−heme peak from Ni^{2+}-HiTrap chromatography are shown in Figure 1. These results indicate that the Hx−heme complex purified by the method described in this report is monomeric. The sedimentation coefficients of the two samples in Figure 1 are very similar but not identical. The early fraction sediments at 4.12 S, and the late fraction sediments at 4.05 S with confidence intervals for S of 4.10−4.13 and 4.04−4.07, respectively, calculated with the discrete species model of SEDFIT. The molecular masses of the complex in these two fractions are estimated to be 56.2 and 54.6 kDa, respectively, through transformation of the $c(s)$ distributions into the $c(M)$ distribution. This transformation assumes the same partial specific volume (0.702 mL/g) for both fractions of the protein and the frictional coefficient (f/f_0 = 1.43) obtained with SEDFIT. This frictional coefficient is consistent with a slightly elongated protein structure such as that defined by crystallographic analysis of the Hx−heme complex (*8*). This analysis is consistent with the conclusion that the Hx−heme fractions represent two Hx−heme species with different, noninterconverting conformational states of Hx or that the Hx in these samples exhibit slight differences in mass that reflect differences in glycosylation.

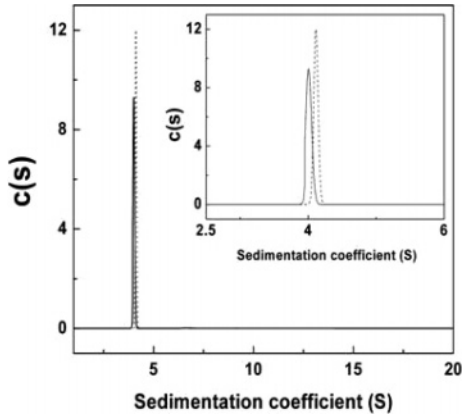

FIGURE 1: Analytical ultracentrifugation analysis of hemopexin using sedimentation velocity. An early-eluting fraction (dashed line) and a late-eluting fraction (solid line) of the Hx−heme peak from the Ni^{2+}-HiTrap column are represented. The inset is an expansion of the low-S region. The Hx−heme concentration is 6.5 μM, in sodium phosphate buffer (20 mM, pH 7.2).

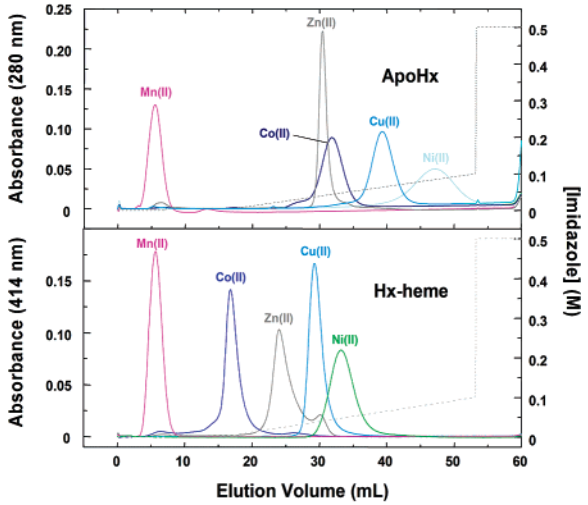

FIGURE 2: Affinity of Hx for immobilized metal ions. Elution profiles of apoHx (top panel) and the Hx−heme complex (bottom panel) generated using an Äkta Purifier and a 5 mL HiTrap chelating HP column (Amersham) charged with various metal ions. Columns were developed with an imidazole gradient (dashed line) in 20 mM sodium phosphate buffer containing 500 mM NaCl at pH 7.4 with a flow rate of 5 mL/min at 25 °C. Each injection contained 0.2 mg of Hx in 2 mL.

Affinity of Human Hx for Metal Chelate Resins. The affinity of our Hx for various metal ions was assessed initially by comparing retention on HiTrap columns charged with various metal ions. All protein samples were stripped of metal ions with EDTA and exchanged into buffer B by ultrafiltration prior to chromatographic analysis. The retention of apoHx by M^{2+}-HiTrap columns observed in these experiments is shown in the top panel of Figure 2. This analysis indicates affinities of apoHx for chelated metal ions in the following order: Ni^{2+} > Cu^{2+} > Co^{2+} > Zn^{2+} > Mn^{2+}.

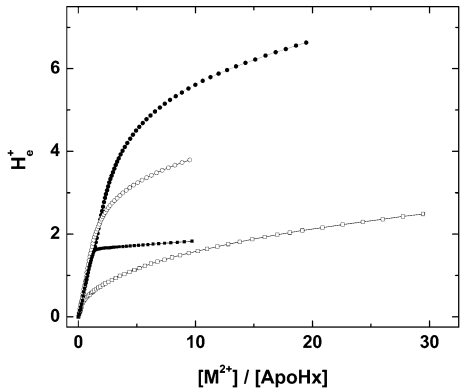

FIGURE 3: Potentiometric titration data for the addition of selected metal ions to apoHx (25 °C, 50 mM NaCl, and pH 7.00). H^+_e is the net number of protons released upon addition of a standard solution of metal ion: (●) Zn^{2+}, (○) Ni^{2+}, (■) Mn^{2+}, and (□) Co^{2+}. For clarity, every other point is not shown; the lines have no numerical significance.

The same analysis performed with the Hx−heme complexes demonstrated that the binding of heme to apoHx decreased the retention of the protein to the HiTrap resin for all metal ions considered. This result suggests that heme binding alters the metal ion binding site(s) responsible for interaction with the metal-charged HiTrap column. Retention times for the Hx−heme complex followed the pattern shown here: Ni^{2+} > Cu^{2+} > Zn^{2+} > Co^{2+} > Mn^{2+} (Figure 2, bottom panel). Note that the binding of heme to apoHx reverses the order of elution from Co^{2+}- and Zn^{2+}-HiTrap columns. The presence of minor components in the elution profile suggests heterogeneity in binding of the protein to the resin, which, again, is most apparent for Co^{2+} and Zn^{2+}.

Potentiometric Analysis of Metal Ion Binding to Hx. Potentiometric titrations were performed to characterize metal ion−Hx interactions further. Titrations of apoHx with Zn^{2+}, Ni^{2+}, Mn^{2+}, and Co^{2+} (pH 7.0) are shown in Figure 3. Consistent with the chromatographic results (Figure 2), these data demonstrate that all of the metal ions studied here bind to apoHx, but the order of elution from the metal affinity chelate resin is not predicted by the titration data. With the exception of the data for Mn^{2+}, these data cannot be fit adequately with models that assume either one or two independent binding sites, suggesting the presence of more than two binding sites. The differential behavior of metal ion binding is most dramatic with Mn^{2+}, which had shown minimal interaction with apoHx during the Mn^{2+}-HiTrap chromatography experiments. In the potentiometric titrations (Figure 3), Mn^{2+} binding to apoHx exhibits a high-affinity binding site with a K_A of $(15 \pm 3) \times 10^6$ M^{-1} and weak site(s) with an estimated affinity of $\leq 2 \times 10^3$ M^{-1}. Potentiometric titrations with Cu^{2+} could not be conducted under the conditions used in Figure 3 because of deprotonation of water coordinated to the metal ion. Even at pH 6.5 (50 mM KNO_3) instability in the pH readings made analysis of the potentiometric titrations unreliable with this metal ion (data not shown).

The effect of heme binding on the metal ion affinity of Hx is shown in Figure 4. These data suggest that heme binding reduces the capacity and/or affinities of Hx for metal ion binding. The proton release observed upon metal ion binding to the Hx−heme complex probably arises from interactions at numerous weak sites.

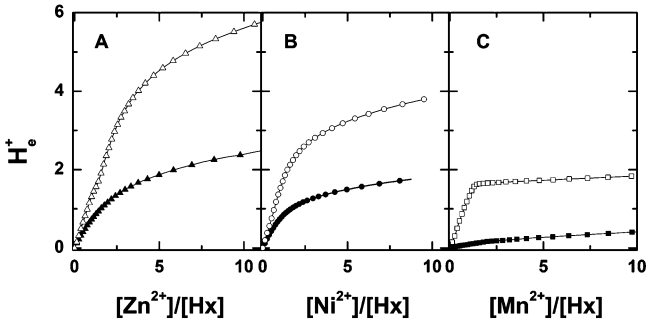

FIGURE 4: Effect of heme on metal ion binding affinity. Proton release upon metal ion binding to apoHx (empty symbols) or the Hx-heme complex (filled symbols) is shown for (A) Zn^{2+}, (B) Ni^{2+}, and (C) Mn^{2+}. For clarity, every other point is not shown; the lines have no numerical significance. Conditions: pH 7.00, 25 °C, and 50 mM NaCl.

NMR Studies of Metal Ion Binding to ApoHx. Information about the type of ligands involved in Ni^{2+} binding to apoHx was sought using proton NMR spectroscopy. Spectra of apoHx in 100% D_2O had no resonances outside the 0−10 ppm region and were similar to spectra reported previously for rabbit Hx (*34*). The addition of Ni^{2+} to apoHx in a 90% H_2O/10% D_2O mixture resulted in the appearance of broad resonances with chemical shifts of ∼125, ∼90, ∼65, and ∼30 ppm (Figure 5A). All four peaks appeared after the addition of 1 equiv of Ni^{2+} per Hx, but their relative intensities changed with an increase in Ni^{2+} concentration, indicating occupation of multiple binding sites with different binding affinities. When the temperature was increased from 25 to 37 °C, the spectrum of a sample of apoHx in a 90% H_2O/10% D_2O mixture containing 2 equiv of Ni^{2+} per Hx changed. All the signals broadened, though differentially, leading to an apparent reduction in peak intensities (Figure 5B). Significantly, the signal at ∼65 ppm split into two, showing that it arises from overlapping peaks with different temperature dependencies. Variation of the temperature between 10 and 42 °C did not lead to a clear splitting of any other signal (not shown), though lines were broader at the higher temperatures. In approximately 100% D_2O, apoHx containing 1 equiv of Ni^{2+} exhibited a substantially reduced intensity for the overlapping signals at ∼65 ppm, indicating that they arise from protons that can be exchanged with solvent deuterons (Figure 5B). The other signals were not significantly affected by the solvent exchange after exposure to D_2O for 72 h, consistent with them corresponding to paramagnetically shifted CH protons. Addition of 0.9 equiv of hemin to apoHx in a 90% H_2O/10% D_2O mixture containing 3 equiv of Ni^{2+} yielded a spectrum essentially the same as the top trace of Figure 5A after the sample had been left for 16 h. Heme binding to this sample of Hx and the absence of unbound heme were confirmed by electronic absorption spectroscopy and by ^1H NMR spectroscopy (not shown). The NMR approach is relatively straightforward because paramagnetically shifted heme resonances of the Hx−heme complex do not overlap the resonances shifted by Ni^{2+} (*34*, *35*).

Co^{2+} binding to apoHx was investigated in a more limited set of NMR experiments than those for Ni^{2+} binding. With 2−4 equiv of Co^{2+} per Hx in 100% D_2O at 37 °C, extremely broad signals were detected at approximately 135, 50, and −50 ppm (data not shown), confirming that Co^{2+} binds to Hx as indicated by the potentiometric data.

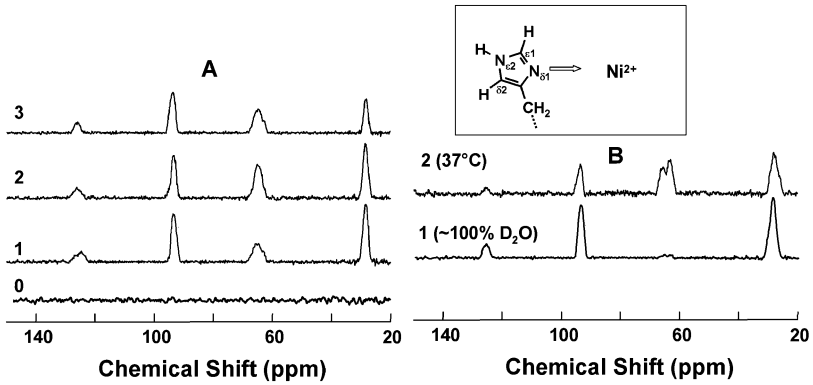

FIGURE 5: ^{1}H NMR spectrum (500 MHz) of the downfield-shifted signals of apoHx. (A) Hx in a 90% H_2O/10% D_2O mixture with 50 mM NaCl, at pH 7 and 25 °C, containing 0, 1, 2, or 3 equiv of Ni^{2+} as indicated; (B) Hx in a 90% H_2O/10% D_2O mixture and 50 mM NaCl containing 2 equiv of Ni^{2+} at 37 °C (top trace). Hx in 100% D_2O and 50 mM NaCl (pH 7) containing 1 equiv of Ni^{2+} at 25 °C (bottom trace). The inset illustrates the coordination of histidine to Ni^{2+} through $N_{\delta 1}$.

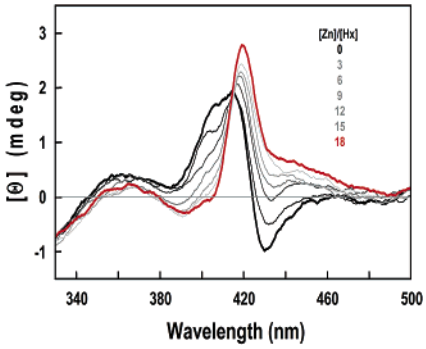

FIGURE 6: Effect of Zn^{2+} binding on the CD spectrum of the Hx−heme complex: the Hx−heme complex (thick black curve), additions of 3−15 equiv of Zn^{2+} (thin black curve), and addition of 18 equiv of Zn^{2+} (red curve). The Hx−heme concentration is 8 μM, with 50 mM bisTris buffer and 50 mM sodium chloride (pH 7.0, 25 °C).

Similar NMR studies were not carried out with Zn^{2+} or Mn^{2+} because the former is diamagnetic, and thus does not shift resonances outside of the diamagnetic envelope of 0−10 ppm, and while the latter is paramagnetic, its magnetic properties cause resonances to broaden substantially rather than shift (*36*).

Circular Dichroism Spectroscopy. The influence of metal ions on the heme binding site of hemopexin was evaluated by determining the Soret-CD spectrum of the Hx−heme complex in the presence and absence of metal ions. While addition of up to 18 equiv of Co^{2+}, Mn^{2+}, and Ni^{2+} has only a minor effect on this region of the CD spectrum, addition of comparable amounts of Cu^{2+} and Zn^{2+} converts the bisignate line shape of this spectrum into a positive Cotton effect (Figure 6) that reverts to the bisignate spectrum upon addition of EDTA.

DISCUSSION

The binding and transport of metal ions by proteins present in blood plasma are major factors in the maintenance of metal ion homeostasis. While the metal ion binding properties and transport roles of albumin (*37*) and transferrin (*38*, *39*) have been studied extensively, the possible contributions of other plasma proteins [e.g., ceruloplasmin (*40*) and histidine-rich glycoprotein (*41*, *42*)] are recognized but less well defined. The abundance of albumin in plasma ensures this protein will dominate metal ion transport, but less abundant proteins may also participate at least transiently in metal ion binding or exchange processes. The fact that many potential metal ion binding proteins of plasma, including hemopexin, are acute phase reactant proteins (*43*) means that their concentrations will increase as the need arises and argues for an essential role for them in minimizing the potential toxicity of metal ions released to blood as the result of various disease processes.

As described above, all hemopexin samples purified in this work were from cryosupernate prepared from single donors. Thus, the chromatographic heterogeneity observed here is the result of the well-recognized microheterogeneity of hemopexin reported previously (*32*). Some previous reports have described hemopexin preparations with components having a mass that is consistent with the formation of dimers or trimers (*27*−*30*). Sedimentation velocity analysis of the hemopexin purified by the method developed in our study fails to detect hemopexin species of a mass greater than that expected from the amino acid sequence and variable carbohydrate content of the protein. As hemopexin possesses three disulfide bonds in the N-terminal domain and three in the C-terminal domain, it seems likely that the larger forms of hemopexin observed in some previous studies result from aggregation caused by disulfide exchange reactions that are promoted by the more strenuous conditions to which many other methods subject the protein during purification. From our results, the spontaneous formation of larger hemopexin species *in vivo* seems unlikely.

By far, the most common use of metal affinity chelate chromatography is for the purification of proteins with the ability to bind metal ions, and frequently, this functional attribute is the result of incorporating a poly-His sequence at one end of recombinantly expressed proteins. In the case of human Hx, the intrinsic metal ion binding capability of the protein was sufficient to allow development of an efficient purification protocol that also took advantage of the differential affinities of metal ion binding proteins of plasma cryosupernate to afford a highly purified product. Less commonly, metal affinity chelate chromatography has been used as an analytical technique to characterize the metal ion binding properties of proteins. Two studies, for example, compared the retention of several proteins to assess protein surface properties and the roles of surface His, Cys, and Trp residues in retention by such resins (*44*, *45*). The results of these studies emphasized the crucial role of surface His

residues in binding of metal ions in general and in the binding of Cu^{2+} and Ni^{2+} in particular. Our findings that human Hx, which possesses 19 His residues, is best retained by immobilized Cu^{2+} and Ni^{2+} and that sequestration of at least two of these His residues through binding of heme diminishes the retention of the protein to these immobilized metal ions are consistent with these previous studies. Notably, the order of elution from immobilized Co^{2+} and Zn^{2+} is reversed with the addition heme, an observation that presumably reflects a significant but undefined change in the accessibility of potential protein surface ligands that accompanies the binding of heme. The minor components noted above that are observed most clearly in the elution of the Hx−heme complex from immobilized Co^{2+} and Zn^{2+} columns provide evidence for more than one binding site for these metal ions at least. Better understanding of the structural basis for these observations will require structure determination of human Hx with metal ions bound.

NMR Studies of Ni^{2+} Binding to the Hx−Heme Complex. The initial characterization of the metal ion binding properties of human hemopexin provided by our work raises the question of where the metal ion binding sites of hemopexin are located and what the relative affinities of these sites for various metal ions are. Human hemopexin is an acidic protein [pI ~5.5−6.4 (see the Results)] with 19 histidyl residues, so the availability of carboxyl and imidazole groups to serve as ligands for metal ion binding is not a limitation. The structure of rabbit hemopexin suggests possible structural origins for linkage between metal ion and heme binding to this protein. For example, two His residues (His213 and His266[2]) provide ligands to the heme iron. In addition, His223 and His272 form H-bonds with heme propionate 6, and His254 is nearby. Other His residues (His56, His217, and His225) are located in the vicinity of the heme binding site, and many others are on the surfaces of the N- and C-terminal domains in positions that face each other in the three-dimensional structure of the rabbit protein. To the extent that the binding of heme may bring these surfaces of the two domains closer together, the involvement of these residues in binding metal ions could differ in apoHx and the Hx−heme complex.

While detailed characterization of the metal ion binding sites of human hemopexin is beyond the scope of this study, our initial NMR studies provide evidence concerning the nature of residues involved in the binding of Ni^{2+} to hemopexin. Inner sphere ligands to Ni^{2+} can occur in a variety of geometries, not all of which lead to paramagnetic Ni^{2+}. The observation of hyperfine-shifted resonances of Ni^{2+}-containing Hx clearly shows, however, that Ni^{2+} bound to Hx is paramagnetic, consistent with either tetrahedral or octahedral geometry. The two exchangeable resonances at ~65 ppm (Figure 5) provide strong evidence for at least two histidyl residues coordinated to Ni^{2+}. For His coordinated through $N_{\delta 1}$, the $N_{\epsilon 2}$ proton would be sufficiently far from the Ni^{2+} not to be broadened beyond detection (inset of Figure 5), and the $N_{\delta 1}$ proton would similarly be detectable for His coordinated through $N_{\epsilon 2}$. No other amino acid residue is likely to have an exchangeable signal shifted so far downfield by paramagnetic Ni^{2+} ions. The resonances at ~125 and ~90 ppm cannot be exchanged with D_2O and probably arise from CH groups of ligands coordinated to Ni^{2+}. On the basis of studies of other Ni^{2+}-substituted proteins (*36*, *46*−*50*), ligands that could give rise to these signals are (a) the $C_{\delta 2}$ protons of His residues coordinated to Ni^{2+} through $N_{\delta 1}$ (inset of Figure 5), (b) the β-CH/γ-CH protons of coordinated Asp or Glu residues, and (c) the γ- and ϵ-protons of Met. We do not include the β-protons of Cys in this list because all Cys residues of Hx participate in disulfide bonds.

Unlike other Ni^{2+}-containing proteins that have been characterized by NMR spectroscopy, Hx contains sialic acid groups. Thus, we considered whether the NMR signals between 130 and 20 ppm resulting from Ni^{2+} binding to Hx (Figure 5) could arise from interaction of Ni^{2+} with sialic acid. Saladini and colleagues (*51*) have reported that *N*-acetylneuraminic acid (NANA), the principal sialic acid in humans, binds Cd^{2+} and Co^{2+} through its carboxylate group and pyranosidic oxygen and that bonding interactions between the acetamido group, which contains a potentially exchangeable NH group, and the bound metal ions do not occur. This result suggests that any paramagnetic perturbation to the chemical shift of the acetamido NH group of Ni^{2+}-bound NANA would have to be a dipolar effect because scalar interactions are rapidly attenuated by bonding frameworks constructed of σ-bonds alone. Without knowledge of the magnetic susceptibility tensor, dipolar chemical shift perturbations cannot be calculated (*36*). However, we can estimate the likely dipolar shifts experienced by an NH group of Ni^{2+}-bound NANA from the study of Ni^{2+}-containing azurin (*49*). The Ni^{2+} of Ni^{2+}-bound azurin is likely to have a greater anisotropy to its magnetic susceptibility than Ni^{2+}-bound NANA because the latter will not be constrained to adopt the low symmetry of the site in azurin. Even with protons close to the Ni^{2+} and lying on the main axes of the magnetic susceptibility tensor, the calculated dipolar chemical shift perturbations of 3−17 ppm (*49*) are considerably smaller than the 55 ppm required to account for the chemical shifts of the exchangeable resonances of Ni^{2+}-bound Hx (Figure 5).

Effect of Cu^{2+} and Zn^{2+} on the Soret-CD Spectrum. The UV−CD spectrum of the human Hx−heme complex studied here exhibits no change upon addition of Cu^{2+} or Zn^{2+} ions and, thus, no effect of metal ion binding on the secondary structure of the protein. While the Soret-CD spectrum exhibited no change upon addition of Co^{2+} or Ni^{2+}, addition of Cu^{2+} or Zn^{2+} changed the Soret-CD spectrum from a bisignate line shape to a positive Cotton effect, and this change could be reversed by the addition of EDTA. Previously reported Soret-CD spectra for various species of the Hx−heme complex indicate that rat and rabbit Hx−heme complexes exhibit a positive Cotton effect while the human protein exhibits a bisignate spectrum (*52*), although an earlier report (*53*) indicated a positive Cotton effect for the human protein.

The origin of the species-specific variation in the Soret-CD spectrum of the Hx−heme complex is most simply explained by the variation in sequence and length of the peptide linking the N- and C-terminal domains of Hx. For rabbit Hx, the heme ligand His213 is present in this peptide, so variations in the coordination geometry of the corresponding residue in other species of Hx could contribute to species-specific spectroscopic properties. In some species (e.g., human), at least one additional His residue and an additional

[2] All sequence numbers used in this report refer to rabbit Hx.

glycosylation site occur in the hinge peptide, so for these species of Hx, alternative axial ligands may be possible, and the preference for one axial His or another may vary with solution conditions. For this change in spectrum to result from a change in His ligand, a structural change in the heme prosthetic group is apparently required. Blauer et al. (*54*) have provided evidence from studies of model heme proteins and heme peptides that bisignate heme Soret-CD spectra reflect distortion of a heme pyrrole ring from planarity with the rest of the heme or the distortion of heme vinyl geometry and do not result from alterations in axial ligand geometry. Some other mechanisms by which **t**he Soret-CD spectrum may be influenced seem unlikely. For example, the crystallographically determined structure that is available provides no evidence for heme orientation disorder, and the extensive hydrogen bonding interactions of the heme propionates mitigate against efficient exchange of the heme with the putative heme binding site that has been proposed (*55*) for the N-terminal domain of the protein. The clear monomeric character of the protein studied in this report argues against a contribution from dimerization- or aggregation-induced exciton coupling of heme groups to the variation in Soret-CD spectrum observed here, as do the bisignate Soret-CD spectra reported for ferricytochromes b_5 (*56*) and *c* (*57*), both of which are known to be monomeric.

The mechanism by which Cu^{2+} or Zn^{2+} induces changes in the Soret-CD spectrum of the Hx−heme complex is not clear, but it could involve (a) binding in the vicinity of the heme binding site with a resulting electrostatic perturbation of the heme environment caused by the presence of the charged metal ion that is sensed only by the Soret-CD spectrum, (b) exchange of one of the axial ligands to the heme iron for another His residue that is near the heme binding site, or (c) perturbation of an electronic interaction between an adjacent Trp or Tyr residue and the heme group. The fact that binding of some metal ions induces this spectroscopic effect while the binding of others does not presumably indicates the inequivalence of binding sites for various metal ions.

Possible Implications of Metal Ion Binding to the Hx−Heme Complex. As discussed above, the ability of hemopexin to bind metal ions raises the clear possibility that this protein participates in some manner in the transport of metal ions in blood or in the exchange of metal ions between proteins. Presumably, such a role would be more significant for apoHx because it exhibits the greater affinity or capacity for metal ions and because the Hx−heme complex should not remain in plasma long prior to its removal by the liver. The possibility that the binding of metal ions such as Cu^{2+} and Zn^{2+} could promote a change in axial ligation raises the further possibility that these or other metal ions may participate in the dissociation of the Hx−heme complex.

ACKNOWLEDGMENT

We thank Prof. David Chen (Department of Chemistry, University of British Columbia) for access to the Beckman-Coulter ProteomeLab PF2D system and Dr. Mark Okon for assistance in NMR data acquisition.

REFERENCES

1. Smith, A., and Morgan, W. T. (1978) Transport of heme by hemopexin to the liver: Evidence for receptor-mediated uptake, *Biochem. Biophys. Res. Commun. 84*, 151−157.
2. Smith, A., and Morgan, W. T. (1979) Haem transport to the liver by haemopexin. Receptor-mediated uptake with recycling of the protein, *Biochem. J. 182*, 47−54.
3. Gutteridge, J. M. (1995) Lipid peroxidation and antioxidants as biomarkers of tissue damage, *Clin. Chem. 41*, 1819−1828.
4. Grinberg, L. N., O'Brien, P. J., and Hrkal, Z. (1999) The effects of heme-binding proteins on the peroxidative and catalatic activities of hemin, *Free Radical Biol. Med. 27*, 214−219.
5. Tolosano, E., and Altruda, F. (2002) Hemopexin: Structure, function, and regulation, *DNA Cell Biol. 21*, 297−306.
6. Delanghe, J. R., and Langlois, M. R. (2001) Hemopexin: A review of biological aspects and the role in laboratory medicine, *Clin. Chim. Acta 312*, 13−23.
7. Morgan, W. T., and Smith, A. (2000) Binding and transport of iron-porphyrins by hemopexin, *Adv. Inorg. Chem. 51*, 205−241.
8. Paoli, M., Anderson, B. F., Baker, H. M., Morgan, W. T., Smith, A., and Baker, E. N. (1999) Crystal structure of hemopexin reveals a novel high-affinity heme site formed between two β-propeller domains, *Nat. Struct. Biol. 6*, 926−931.
9. Smith, A. (2000) Links between cell-surface events involving redox-active copper and gene regulation in the hemopexin heme transport system, *Antioxid. Redox Signal. 2*, 157−175.
10. Wu, M. L., and Morgan, W. T. (1993) Characterization of hemopexin and its interaction with heme by differential scanning calorimetry and circular dichroism, *Biochemistry 32*, 7216−7222.
11. Wu, M. L., and Morgan, W. T. (1995) Thermodynamics of heme-induced conformational changes in hemopexin: Role of domain-domain interactions, *Protein Sci. 4*, 29−34.
12. Pasternack, R. F., Gibbs, E. J., Mauk, A. G., Reid, L. S., Wong, N. M., Kurokawa, K., Hashim, M., and Müller-Eberhard, U. (1985) Kinetics of hemoprotein reduction and interprotein heme transfer, *Biochemistry 24*, 5443−5448.
13. Porath, J., and Olin, B. (1983) Immobilized metal ion affinity adsorption and immobilized metal ion affinity chromatography of biomaterials. Serum protein affinities for gel-immobilized iron and nickel ions, *Biochemistry 22*, 1621−1630.
14. Andersson, L. (1984) Fractionation of human serum proteins by immobilized metal affinity chromatography, *J. Chromatogr. 315*, 167−174.
15. Porath, J., Olin, B., and Granstrand, B. (1983) Immobilized-metal affinity chromatography of serum proteins on gel-immobilized group III A metal ions, *Arch. Biochem. Biophys. 225*, 543−547.
16. Jensen, P. E. H., Birkenmeier, G., and Stigbrand, T. (1991) Zinc chelates bind human hemopexin, *Acta Chem. Scand. 45*, 537−538.
17. Mantovaara, T., Pertoft, H., and Porath, J. (1991) Further characterization of carboxymethylated aspartic acid agarose. Purification of human α-2-macroglobulin and hemopexin, *Biotechnol. Appl. Biochem. 13*, 371−379.
18. de Monti, M., Miot, S., Le Goff, P., and Duval, J. (1998) Characterization of trout serum hemopexin through the use of a recombinant protein, *C. R. Seances Acad. Sci., Ser. III 321*, 299−304.
19. Cham, B. E., and Knowles, B. R. (1976) A solvent system for delipidation of plasma or serum without protein precipitation, *J. Lipid Res. 17*, 176−181.
20. Seery, V. L., Hathaway, G., and Müller-Eberhard, U. (1972) Hemopexin of human and rabbit: Molecular weight and extinction coefficient, *Arch. Biochem. Biophys. 150*, 269−272.
21. Schuck, P. (2000) Size-distribution analysis of macromolecules by sedimentation velocity ultracentrifugation and Lamm equation modeling, *Biophys. J. 78*, 1606−1619.
22. Laue, T. M., Shah, B. D., Ridgeway, T. M., and Pelletier, S. L. (1992) in *Analytical Ultracentrifugation in Biochemistry and Polymer Science* (Harding, S. E., Rowe, A. J., and Horton, J. C., Eds.) pp 90−125, Royal Society of Chemistry, London.
23. Laskowski, M., and Finkenstadt, W. R. (1972) Study of protein−protein and of protein−ligand interactions by potentiometric methods, *Methods Enzymol. 26*, 193−277.
24. Mauk, M. R., Barker, P. D., and Mauk, A. G. (1991) Proton linkage of complex formation between cytochrome *c* and cytochrome b_5: Electrostatic consequences of protein−protein interactions, *Biochemistry 30*, 9873−9881.
25. Mauk, M. R., Ferrer, J. C., and Mauk, A. G. (1994) Proton linkage in formation of the cytochrome *c*−cytochrome *c* peroxidase complex: Electrostatic properties of the high- and low-affinity cytochrome binding sites on the peroxidase, *Biochemistry 33*, 12609−12614.

26. Inubushi, T., and Becker, E. D. (1983) Efficient detection of paramagnetically shifted NMR resonances by optimizing the WEFT pulse sequence, *J. Magn. Reson. 51*, 128−133.
27. van Gelder, W., Huijskes-Heins, I. E., Hukshorn, C. J., de Jeu-Jaspars, C. M., van Noort, W. L., and van Eijk, H. G. (1995) Isolation, purification and characterization of porcine serum transferrin and hemopexin, *Comp. Biochem. Physiol., Part B: Biochem. Mol. Biol. 111*, 171−179.
28. Aisen, P., Leibman, A., Harris, D. C., and Moss, T. (1974) Human hemopexin. Preparation and magnetic properties, *J. Biol. Chem. 249*, 6824−6827.
29. Müller-Eberhard, U., and English, E. C. (1967) Purification and partial characterization of human hemopexin, *J. Lab. Clin. Med. 70*, 619−626.
30. Hrkal, Z., and Müller-Eberhard, U. (1971) Partial characterization of the heme-binding serum glycoproteins rabbit and human hemopexin, *Biochemistry 10*, 1746−1750.
31. Coddeville, B., Stratil, A., Wieruszeski, J. M., Oliver, R. W., Green, B. N., and Spik, G. (1995) Characterization of sheep hemopexin glycovariants, *Glycoconjugate J. 12*, 645−650.
32. Kamboh, M. I., and Ferrell, R. E. (1987) Genetic studies of low-abundance human plasma proteins. VI. Polymorphism of hemopexin, *Am. J. Hum. Genet. 41*, 645−653.
33. Takahashi, N., Takahashi, Y., and Putnam, F. W. (1984) Structure of human hemopexin: *O*-Glycosyl and *N*-glycosyl sites and unusual clustering of tryptophan residues, *Proc. Natl. Acad. Sci. U.S.A. 81*, 2021−2025.
34. Cox, M. C., Le Brun, N., Thomson, A. J., Smith, A., Morgan, W. T., and Moore, G. R. (1995) MCD, EPR and NMR spectroscopic studies of rabbit hemopexin and its heme binding domain, *Biochim. Biophys. Acta 1253*, 215−223.
35. Deeb, R. S., Müller-Eberhard, U., and Peyton, D. H. (1994) Proton NMR study of the heme complex of hemopexin, *Biochim. Biophys. Acta 1200*, 161−166.
36. Bertini, I., and Luchinat, C. (1996) NMR of paramagnetic substances, *Coord. Chem. Rev. 150*, 1−296.
37. Peters, T. (1996) *All About Albumin: Biochemistry, Genetics, and Medical Applications*, Academic Press, San Diego.
38. Testa, U. (2002) *Proteins of Iron Metabolism*, CRC Press, Boca Raton, FL.
39. Chung, J., and Wessling-Resnick, M. (2003) Molecular mechanisms and regulation of iron transport, *Crit. Rev. Clin. Lab. Sci. 40*, 151−182.
40. Zgirski, A., and Frieden, E. (1990) Binding of Cu(II) to non-prosthetic sites in ceruloplasmin and bovine serum albumin, *J. Inorg. Biochem. 39*, 137−148.
41. Morgan, W. T. (1981) Interactions of the histidine-rich glycoprotein of serum with metals, *Biochemistry 20*, 1054−1061.
42. Morgan, W. T. (1985) The histidine-rich glycoprotein of serum has a domain rich in histidine, proline, and glycine that binds heme and metals, *Biochemistry 24*, 1496−1501.
43. Gabay, C., and Kushner, I. (1999) Acute-phase proteins and other systemic responses to inflammation, *N. Engl. J. Med. 340*, 448−454.
44. Hemdan, E. S., Zhao, Y. J., Sulkowski, E., and Porath, J. (1989) Surface topography of histidine residues: A facile probe by immobilized metal ion affinity chromatography, *Proc. Natl. Acad. Sci. U.S.A. 86*, 1811−1815.
45. Sidenius, U., Farver, O., Jons, O., and Gammelgaard, B. (1999) Comparison of different transition metal ions for immobilized metal affinity chromatography of selenoprotein P from human plasma, *J. Chromatogr., B: Biomed. Sci. Appl. 735*, 85−91.
46. Bertini, I., Canti, G., Luchinat, C., and Mani, F. (1981) ^{1}H NMR spectra of the coordination sphere of cobalt-substituted carbonic anhydrase, *J. Am. Chem. Soc. 103*, 7784−7788.
47. Blaszak, J. A., Ulrich, E. L., Markley, J. L., and McMillin, D. R. (1982) High-resolution proton nuclear magnetic resonance studies of the nickel(II) derivative of azurin, *Biochemistry 21*, 6253−6258.
48. Jimenez, H. R., Salgado, J., Moratal, J. M., and Morgenstern-Badarau, I. (1996) EPR and magnetic susceptibility studies of cobalt(II)- and nickel(II)-substituted azurins from *Pseudomonas aeruginosa*. Electronic structure of the active sites, *Inorg. Chem. 35*, 2737−2741.
49. Salgado, J., Jimenez, H. R., Moratal, J. M., Kroes, S., Warmerdam, G. C., and Canters, G. W. (1996) Paramagnetic cobalt and nickel derivatives of *Alcaligenes denitrificans* azurin and its M121Q mutant. A ^{1}H NMR study, *Biochemistry 35*, 1810−1819.
50. Hannan, J. P., Davy, S. L., Moore, G. R., Eady, R. R., and Andrew, C. R. (1998) Effect of nickel(II) substitution on the resonance Raman and NMR spectra of *Alcaligenes xylosoxidans* azurin II: Implications for axial-ligand bonding interactions in cupredoxin active sites, *J. Biol. Inorg. Chem. 3*, 282−291.
51. Saladini, M., Menabue, L., and Ferrari, E. (2002) Binding ability of sialic acid towards biological and toxic metal ions. NMR, potentiometric and spectroscopic study, *J. Inorg. Biochem. 88*, 61−68.
52. Shipulina, N., Smith, A., and Morgan, W. T. (2000) Heme binding by hemopexin: Evidence for multiple modes of binding and functional implications, *J. Protein Chem. 19*, 239−248.
53. Morgan, W. T., and Vickery, L. E. (1978) Magnetic and natural circular dichroism of metalloporphyrin complexes of human and rabbit hemopexin, *J. Biol. Chem. 253*, 2940−2945.
54. Blauer, G., Sreerama, N., and Woody, R. W. (1993) Optical activity of hemoproteins in the Soret region. Circular dichroism of the heme undecapeptide of cytochrome *c* in aqueous solution, *Biochemistry 32*, 6674−6679.
55. Baker, H. M., Anderson, B. F., and Baker, E. N. (2003) Dealing with iron: Common structural principles in proteins that transport iron and heme, *Proc. Natl. Acad. Sci. U.S.A. 100*, 3579−3583.
56. Singh, H. K., and Wilson, M. T. (1990) Characterization of haem disorder in cytochrome b_5 by circular dichroism, *Biochem. Soc. Trans. 18*, 1272−1273.
57. Myer, Y. P. (1968) Conformation of cytochromes. II. Comparative study of circular dichroism spectra, optical rotatory dispersion, and absorption spectra of horse heart cytochrome *c*, *J. Biol. Chem. 243*, 2115−2122.

BI0481747